JOURNAL OF GEOPHYSICAL RESEARCH, VOL. 103, NO. D15, PAGES 18,981–18,997, AUGUST 20, 1998

On the use of hydrocarbons for the determination of tropospheric OH concentrations

D. H. Ehhalt, F. Rohrer, and A. Wahner

Institut für Atmosphärische Chemie, Forschungszentrum Jülich, Jülich, Germany

M. J. Prather

Department of Earth System Science, University of California, Irvine

D. R. Blake

Department of Chemistry, University of California, Irvine

Abstract. This paper explores a new approach to estimating atmospheric hydroxyl radical concentrations from regional measurements of a suite of hydrocarbons. The approach is guided by the study of a suite of synthetic tracers, i, with uniform continental sources and constant but different lifetimes of 1, 2, 5, 20, 50, and 100 days, whose global distributions are calculated from a three-dimensional chemical tracer model. With the help of the model we show that in a grid box the standard deviation σ_i divided by the average concentration $\overline{M_i}$ is a unique function of the chemical lifetime τ_i. In favorable cases, for instance, in surface air within a specific region sampled by the Pacific Exploratory Mission (PEM) West B campaign, that function takes a simple form: $\sigma_i/\overline{M_i} = A \times \tau_i^{-\alpha}$, with $\alpha = 0.48$, very close to $1/2$. An analogous relation is found for the alkanes, ethane through n-hexane, measured during the PEM West B campaign in the same domain, with their reaction rate constant with OH, k_{OH}. That relation has the form $\sigma_i/\overline{M_i} = B \times (k_{\mathrm{OH},i})^{\alpha'}$, with $\alpha' = 0.49$. Using the alkenes, for example propene, which also react with O_3, the dependence on $k_{\mathrm{OH},i}$ can be related to a dependence on τ_i. This allows us to estimate the OH concentration, $6 \times 10^5 \mathrm{cm}^{-3}$, with an error of roughly a factor of 2 for this region (boundary layer, 30°N-40°N latitude, and 135°E-155°E longitude in March). This estimate is essentially based on empirical relations only and the assumption that the considered hydrocarbons have the same source distribution. As a by-product, we show that the α defined above is related to the slope in the (logarithmic) correlation plot between the mixing ratios of two trace gases with different lifetimes. We also show that the global distribution of α appears to be a useful tool to diagnose fast regional transport.

1. Introduction

The atmospheric distribution of trace gases is governed by three processes, namely, production or emissions (and their geographical distribution), transport, and losses. Each one of these processes leaves its signature on the atmospheric distribution. In turn, measured trace gas distributions can be used to glean information about these three processes. Particularly useful for that purpose are the light hydrocarbons, because they possess similar source and destruction processes yet a large range of destruction rates. Thus they can probe the processes at various timescales. Moreover, the techniques employed usually permit the measurement of a large suite of hydrocarbons from a sample, that is, from the same air parcel. This has allowed a simple conceptual approach to extract information from hydrocarbon measurements, namely, the use of ratios of hydrocarbon concentrations. Appropriate rationing cancels some of the common dependencies (e.g., transport and source distribution) but retains the information on the other process, for example, the chemical loss rates of hydrocarbons. From it the concentration of OH, which is the major removal agent for hydrocarbons, can be eventually derived [see *McKeen et al.*, 1996]. The procedure has the added advantage that its application does not require the measurement of complete hydrocarbon concentration fields but the measure-

Paper number 98JD01106.
0148-0227/98/98JD-01106$09.00.

ment of time series at a few well-selected sites suffice for the purpose. Besides OH in urban, rural, oceanic, and free tropospheric air masses [*Calvert*, 1976; *Singh et al.*, 1981; *Blake et al.*, 1993; *Roberts et al.*, 1984; *Bamber et al.*, 1984; *McKenna et al.*, 1995; *McKeen et al.*, 1996; *Kramp and Volz-Thomas*, 1997], the photochemical age of air masses [*Nelson and Quigley*, 1982; *Roberts et al.*, 1984, 1985; *Rudolph and Johnen*, 1990] and the rate of dilution of polluted boundary layer air with background air [*McKeen et al.*, 1996] have been determined by various methods of rationing hydrocarbons. However, all these applications make a number of simplifying assumptions which introduce possibly large uncertainties in the desired results. So far no studies of these systematic uncertainties have been published, and their magnitude remains unknown.

In this paper we propose an alternative approach to derive OH concentrations from hydrocarbon measurements, an alternative which requires fewer and different assumptions, and thus when combined with the traditional methods, it may provide an indication of the systematic errors involved in estimating OH. In the following we will first describe the assumptions underlying the traditional approach of rationing. We then show that the assumption of diffusive mixing significantly changes the interpretations in some of the hydrocarbon correlations.

Finally, we use a three-dimensional chemical tracer model to derive an empirical relation between the local variance of a suite of tracers and their lifetimes. This relationship points to a new way in which hydrocarbon measurements may be used to derive OH concentrations without assumptions about the underlying physical model of mixing. To remain focused, the study is limited to near-surface air.

2. Use of Hydrocarbon Ratios to Determine OH

The underlying assumption in the rationing concept is that the function, which relates the hydrocarbon mixing ratio at the point of measurement to that of a point upstream, depends only on transport (mixing) and chemical loss and that it can be separated into a product of two terms, one solely depending on transport *T(t,x)* and the other solely depending on chemical loss *L(t,x)* [*McKeen et al.*, 1990]. In all cases a Lagrangian approach is used with the further assumption that the chemical operator, *L(t,x)*, is given by a simple exponential decay in time, that is,

$$M_i(t,x) = M_i(0,x) \times T(t,x) \times e^{-t/\tau_i} \qquad (1)$$

where M_i is the mixing ratio of species i, t is the time since last observation at time zero, x represents the geographical coordinates, and τ_i is the constant chemical lifetime.

In some cases it is also assumed that

$$T(t,x) = e^{-t/\tau} \qquad (2)$$

where τ is the time constant for mixing or dilution with background air of vanishing trace gas concentrations. The vaiable τ is assumed to be the same for all species and independent of the location. [cf. *McKeen et al.*, 1996]. Equation (1) with (2) for the transport function is a solution of the simple differential equation

$$\frac{dM_i}{dt} = -\frac{M_i}{\tau} - \frac{M_i}{\tau_i} \qquad (3)$$

An often used correlation of hydrocarbons species i with species j is the plot of $\ln(M_i)$ versus $\ln(M_j)$. Equation (3) predicts that the correlation curve is linear, with a slope

$$\beta = \frac{1/\tau + 1/\tau_i}{1/\tau + 1/\tau_j} \qquad (4)$$

Such a linear correlation is, indeed, found experimentally [*McKeen et al.*, 1996]. Another often used form is the correlation of the ratio of three hydrocarbon species: $\ln(M_i/M_k)$ versus $\ln(M_j/M_k)$. In this way the common dependence on mixing cancels. The slope of this curve, which is also linear, is

$$\gamma = \frac{1/\tau_i - 1/\tau_k}{1/\tau_j - 1/\tau_k} \qquad (5)$$

If we allow for the fact that the hydrocarbons i, j, and k react exclusively with OH and thus $\tau_i^{-1} = k_i \times [\mathrm{OH}]$, then

$$\gamma = \frac{k_i - k_k}{k_j - k_k} \qquad (6)$$

where k is the rate constant for the reaction of species i, j, and k. Obviously, the simple model makes testable predictions about the correlation of hydrocarbons and of their ratios. If the background air, with which the observed parcel is mixing, has a finite mixing ratio MB instead of zero, the differential equation (3) changes to

$$\frac{dM_i}{dt} = -\frac{M_i}{\tau_i} - \frac{M_i - MB_i}{\tau} \qquad (7)$$

The solution (1) changes to

$$M_i(t) = \frac{MB_i}{1+\tau/\tau_i} + \left[M_i(0) - \frac{MB_i}{1+\tau/\tau_i}\right] \times e^{-t\times(1/\tau+1/\tau_i)} \qquad (8)$$

The introduction of a finite background concentration changes the slopes β and γ considerably, and the curves in general are no longer linear (see *McKeen et al.* [1996] for some special cases and numerical examples).

The physical model underlying differential equations (3) and (7) is that of an air parcel with an initial content of species i being placed at time zero into an infinite reservoir of air with another but constant mixing ratio of species i. Both air masses are thought to be com-

pletely mixed internally and to exchange air between them at a constant rate defined by τ. The time t in (8) and (1) can be replaced by a distance x, if the air parcel moves along a trajectory with the speed v, then $t \rightarrow x/v$. Thus the approach can be used to follow the fate of an air parcel as it sits or moves along in a large reservoir of background air.

Equation (8) allows us to estimate the mixing time τ and the concentration of $[OH] = \tau_i^{-1} \times k_i^{-1}$, if the available set of hydrocarbon data meets certain requirements: namely, (1) that it contains enough clean air data to estimate the background mixing ratios; (2) that the air parcels possess a range of travel times, t, since the last contact with a source and that t can be estimated, for example, by trajectory analysis; (3) that there are at least two species measured with different chemical lifetimes; and (4) that the air parcels encounter no source between time 0 and t.

The approach has the advantage that it is conceptually simple, that it defines useful parameters, and that it yields plausible values for [OH] and τ. *McKeen et al.*, [1996], for example, have used it to derive [OH] and τ from hydrocarbon measurements obtained in the lowermost atmosphere during the Pacific Exploratory Mission (PEM) West A aircraft campaign. As McKeen et al. pointed out, however, there are disadvantages as well. One is that the variance and the errors in the estimates of [OH] and τ resulting from different pairs of hydrocarbons are large; another is that the assignment of background mixing ratios is difficult.

There is, however, also a more fundamental problem. The applicability of the model is limited to situations where the simplifying assumptions are met by atmospheric conditions, at least approximately. Conversely the concept of a two-box model is a highly idealized description of atmospheric dilution. Thus the scientific task is rather to demonstrate (1) where the model assumptions are met or (2) what systematic uncertainties are to be expected when they are met only approximately under the conditions of observations. To highlight this point we first demonstrate that the model predictions about β, γ, and τ_i depend on the model assumptions. To do so, we consider two model cases where the mixing is provided by turbulent diffusion; that is, we contrast the assumption of mixing between the required minimum of two reservoirs with the assumption of gradual mixing along a continuum of reservoirs. This also sets the stage for the later treatment including all modes of transport by a three-dimensional chemical tracer model.

3. One-Dimensional (1-D) Model

We first consider the case of one-dimensional vertical diffusion of a tracer with constant chemical lifetime τ_i. We assume an infinitely extended source at the surface, zero mixing ratio at high altitudes, and a turbulent diffusion coefficient D, which is constant with altitude. We also neglect the vertical gradient in air density, a reasonable assumption for short-lived species. The differential equation for the local material balance at steady state then is

$$\frac{\partial M_i}{\partial t} = D \times \frac{\partial^2 M_i}{\partial z^2} - \frac{M_i}{\tau_i} = 0 \tag{9}$$

with the solution

$$M_i(z) = M_i(0) \times e^{-z/\sqrt{D \times \tau_i}} \tag{10}$$

[see *Bonsang et al.*, 1987]. The characteristic height scale, $\sqrt{D \times \tau_i}$, multiplied by a factor of $\sqrt{2}$, corresponds to the average vertical distance traveled by an air parcel during the chemical lifetime of the tracer. The mixing ratios at the surface, $M_i(0)$, can be calculated from a uniform surface flux J,

$$J = -D \times \left.\frac{\partial M_i(z)}{\partial z}\right|_{z=0} \tag{11}$$

$$J = \frac{D \times M_i(0)}{\sqrt{D \times \tau_i}} \tag{12}$$

and

$$M_i(0) = J \times \sqrt{\frac{\tau_i}{D}} \tag{13}$$

The surface concentration scales as $\sqrt{\tau_i}$ and depends on D; the column-integrated concentration, $J \times \tau_i$, scales as τ_i and is independent of D.

Obviously, (10) does not allow the separation of the dependencies on transport and chemical destruction into two independent factors. This is a consequence of the diffusive transport term in differential equation (9). Other examples are the solutions of the diffusion equations for point and line sources reported by *McKeen et al.* [1990] [cf. *McKenna*, 1997]. Moreover, the chemical lifetime enters (10) as $\sqrt{\tau_i}$ instead of τ_i as in (1), a consequence of the fact that diffusive transport enters as a second derivative in the local balance equation (9). Both of these differences have consequences for the determination of [OH].

Finally, when we calculate the slope for the plot of $\ln(M_i(z))$ versus $\ln(M_j(z))$ we obtain

$$\beta' = \sqrt{\frac{\tau_j}{\tau_i}} \tag{14}$$

independent of the transport parameter, D.

The slope when plotting the ratios of the mixing ratios, $\ln(M_i/M_k)$ versus $\ln(M_j/M_k)$ becomes

$$\gamma' = \frac{\sqrt{1/\tau_i} - \sqrt{1/\tau_k}}{\sqrt{1/\tau_j} - \sqrt{1/\tau_k}} \tag{15}$$

or

$$\gamma' = \frac{\sqrt{k_i} - \sqrt{k_k}}{\sqrt{k_j} - \sqrt{k_k}} \tag{16}$$

when we replace τ_i^{-1} by [OH] $\times$ k_i (see above). The diffusion model also predicts straight lines for the relations of $\ln(M_i)$ versus $\ln(M_j)$ and $\ln(M_i/M_k)$ versus $\ln(M_j/M_k)$. However, when mixing is interpreted in terms of turbulent diffusion instead of exchange between two well-mixed air masses, the slopes for measured hydrocarbon concentrations take on a drastically different meaning from the earlier ones from (4) and (5). Clearly, the predicted numerical values for the slopes β' and γ' are different as well. Interestingly, both 3-D modeled tracers and measured hydrocarbons, show slopes, β', close to $\sqrt{\tau_j/\tau_i}$ within the PEM West domain (see Figure 6). Moreover, γ' is close to $(\sqrt{k_i} - \sqrt{k_k})$ / $(\sqrt{k_j} - \sqrt{k_k})$ for that domain.

4. 2-D Model

4.1. Analytic Solution

The next example approaches one step closer to reality by including horizontal, meridional advection with a wind speed v uniform at all altitudes in addition to vertical eddy diffusion. Again, we assume steady state, a constant vertical eddy diffusion coefficient D a constant chemical lifetime τ_i as well as constant air density. The resulting differential equation is

$$v \times \frac{\partial M_i(y,z)}{\partial y} = D \times \frac{\partial^2 M_i(y,z)}{\partial z^2} - \frac{M_i(y,z)}{\tau_i} \quad (17)$$

It is simple enough to have analytical solutions. With an initial vertical profile of $M_i(0,z) = M_i(0,0) \times e^{-z/\sqrt{D\times\tau_i}}$ (equation (10)) and vanishing surface sources, we obtain the longitude and height dependent solution

$$M(y,z) = \frac{M(0,0)}{2} \times \left(e^{-z/\sqrt{D\tau}} \times \left[1 + \mathrm{erf}\left(\frac{z\tau - 2y\sqrt{D\tau}/v}{2\tau\sqrt{Dy/v}}\right)\right] + e^{+z/\sqrt{D\tau}} \times \left[1 - \mathrm{erf}\left(\frac{z\tau + 2y\sqrt{D\tau}/v}{2\tau\sqrt{Dy/v}}\right)\right]\right) \quad (18)$$

and for the surface mixing ratio we obtain

$$M(y,0) = M(0,0) \times \left[1 - \mathrm{erf}\left(\sqrt{y/(v\times\tau_i)}\right)\right] \quad (19)$$

where the error function $\mathrm{erf}(x') = 2/\sqrt{\pi} \times \int_0^{x'} e^{-x^2/2} dx$.

Equation (19) may be viewed as the surface distribution of a tracer in air flowing from a large polluted continent out over a large emission free ocean. It too depends on $\sqrt{\tau_i}$ rather than τ_i. Except for the initial mixing ratio $M_i(0,0)$ (see (13)), (19) does not depend on D.

The solution of differential equation (17) does, however, strongly depend on the vertical profile established over the emission region. With an initial vertical profile of constant mixing ratio the solution at the surface would have taken the form

$$M(y,0) = M(0,0) \times e^{-y/(v\times\tau_i)} \quad (20)$$

This solution clearly depends on the chemical lifetime rather than on its square root, and the dependence can be readily factored into a form like (1) considering that $t = y/v$.

4.2. A Numerical Example

A case somewhat more applicable to atmospheric observations, that of an air mass contained in the northern midlatitude westerlies circling the globe across two continents separated by two oceans, lends itself to numerical solution. The longitudes of the continents are selected to represent the Eurasian and North American continent (and the Atlantic and Pacific Oceans) at 40° latitude. The uniform wind speed, v = 8 m s^{-1}, corresponds to the climatological mean at that latitude during spring. The air mass circles the globe once in 40 days. The vertical eddy diffusion coefficient D is 20 m^2 s^{-1}. The continents act as source with uniform surface emission rates of 10^{14} molecules m^{-2} s^{-1} for each of the three synthetic tracers Rn5, Rn20, and Rn100, with constant lifetimes τ_i of 5, 20, and 100 days. The oceans have zero emissions (see Figure 1d). There is no surface deposition of the tracers. The mixing ratio is set to zero at the upper boundary (100 km). As long as the upper boundary is located high above the surface, the actual height of the boundary is of little influence on the surface concentrations. Steady state was reached by allowing a spin up of 400 days corresponding to 10 cycles of the air mass around the globe, and thus results do not depend on initial profiles.

The surface mixing ratios for each of the three tracers along the longitude circle is shown in Figure 1. They exhibit some interesting features, namely, the decrease in mixing ratio when the air moves out over the ocean is nonexponential; the rate of decrease is much faster in the first 5° of longitude downwind of the continents as evidenced by the curvature of the decay curves on a log scale. By the same token the increase when moving over the continent is much faster than the function $(1 - e^{-t/\tau})$. Maximum concentrations are reached at the end of the travel over the continents. Only in the case of Rn5 and the broad Eurasian continent do the surface concentrations approach the steady state value for an infinitely extended source indicated by the dotted lines in Figure 1. These asymptotes are proportional to $\sqrt{\tau_i}$, not τ_i (see (13)). For other conditions the lifetimes are too long compared to the travel time over the continents to reach steady state, but their maximum values (reached over the continents) are also roughly proportional to $\sqrt{\tau_i}$.

The fast decay in the surface concentration as the air moves out over the ocean can be easily understood when we remind ourselves that differential equation (17)

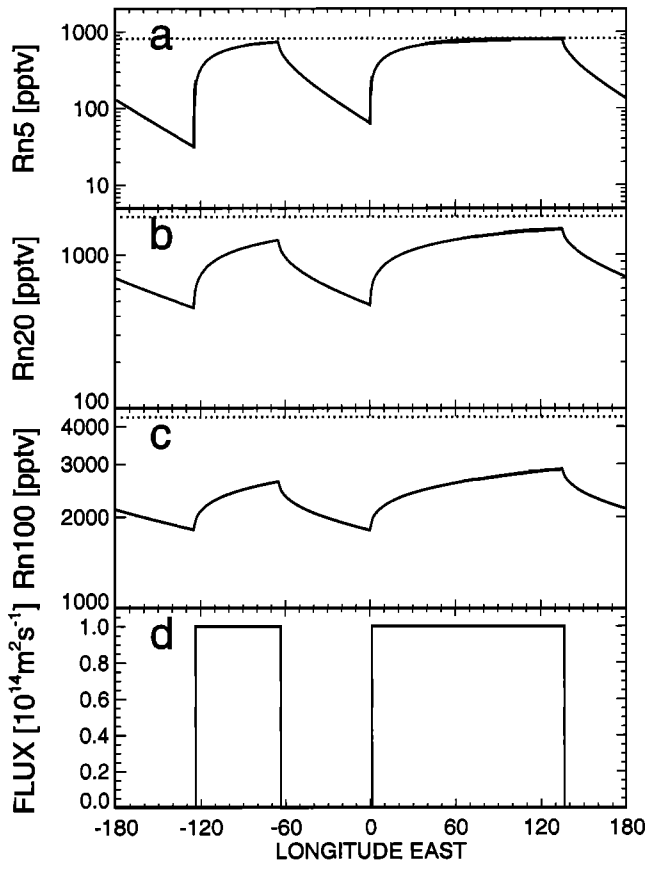

Figure 1. Surface mixing ratios of the synthetic tracers (a) Rn5, (b) Rn20, and (c) Rn100 as a function of longitude at 30°N-40°N latitude during March calculated from a two-dimensional (2-D) advection diffusion model. The dotted lines indicate the asymptotic mixing ratios reached after travel over a continent of infinite longitudinal extent. (d) Position of the continental sources and the emission flux.

can also be viewed as describing a Lagrangian air parcel, in the sense that the whole vertical column of air moves with the same speed. There is no mixing in the horizontal direction. As the column moves out over the ocean and is no longer replenished from below, the total amount of tracer in the column decays as e^{-t/τ_i} (or since $y = v \times t$ as $e^{-y/(v\times\tau_i)}$). However, at the same time, diffusion dramatically changes the vertical distribution of the tracer. Coming off the continent, the mixing ratio is highest in the surface layer, and vertical mixing reduces this gradient. Combining the removal by chemical decay with this upward transport by diffusion, the total decrease in the near-surface region is much faster than predicted by the chemical loss alone.

The relative vertical redistribution is shown as a sequence of Rn5 profiles in Figure 2, spaced over steps of 1 day (691 km in longitudinal travel). We have scaled out the chemical decay through multiplying by $e^{+t/\tau}$. Since Rn5 is relatively short-lived, its vertical distribution when leaving the Eurasian continent is very close to its steady state distribution (equation (10)), that is, a straight line on a log scale. During the early period of travel over the ocean, vertical transport alone reduces the surface concentration of Rn5 quite fast, a factor of 2.4 in the first 5 days, apparently doubling the initial removal rate over that by chemical loss alone. At higher altitudes, transport adds tracer, slowing the decrease in concentration away from the continents expected from chemical decay alone. The altitude of the compensation point (i.e., zero change) is in the middle troposphere, shifts upward with time for this case, and is the only place where the tracer decays according to its chemical lifetime.

Over the oceans that are crossed in at most 11 days, however, a uniform vertical profile is never reached, and vertical transport will always make significant contribution to the change in surface concentration, even for Rn5. Figures 1 and 2 demonstrate quite clearly that the rate of dilution is not constant in time or space, as is assumed in (1) and (8). It changes considerably not only over large distances but also over short intervals when leaving the coast. It is the coupling between chemistry and transport that sets up the large-scale vertical gradients over the source regions and thus controls the initial dilution off the coast, which is driven by diffusion in this model. Thus even the rapid, early dilution of air from continental sources depends on the rate of chemical loss of the tracer.

4.3. Tracer-Tracer Correlations

It is instructive to look at the slope β from the variation of $\ln(\mathrm{Rn}_i)$ versus $\ln(\mathrm{Rn}_j)$ from this 2-D example

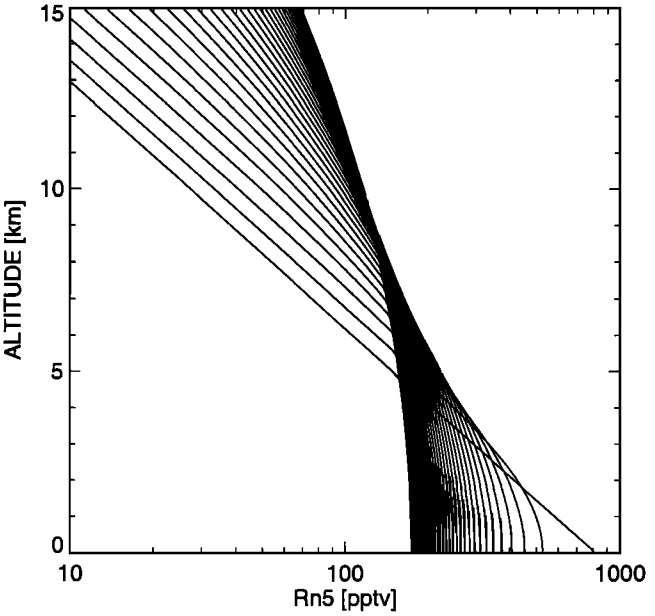

Figure 2. Temporal redistribution of the vertical Rn5 mixing ratio after leaving the Eurasian continent and moving over an infinite ocean. The profiles present the effect of vertical transport only (see text) and are given in time steps of 1 day beginning with the profile of the highest surface value.

as shown in Figure 3. An interval of 10° longitude is used to generate the tracer variations from which β is derived. We choose Rn_j to be the longer lived of the two tracers. This interval averages over the discontinuities in slope at the coasts (see Figure 1), and therefore the portions of the curves within ±10° from the coasts are disregarded.

As Figure 3 indicates, β is reset by the differential equations to a value approximating $\sqrt{\tau_j/\tau_i}$ (dashed lines) every time the air mass crosses the upwind or downwind coasts of the continent. This behavior is indicated exactly by the analytic solution above (equation (19)). Over the continents, β decreases asymptotically toward zero because of the fact that the shorter-lived tracer approaches steady state faster, while the concentration of the longer-lived tracer is still increasing (see Figure 1). Over the ocean, β increases and would eventually reach a value τ_j/τ_i, but, given the lifetimes considered here and the air mass travel time of at most 11 days over the ocean, that value is not reached. Thus the possible total range for β, 0 to τ_j/τ_i, is not assumed for the lifetimes and latitude considered in our 2-D example. Because β is reset to a value $\sqrt{\tau_j/\tau_i}$ at every transition of the air mass over the continental margins, the range is significantly reduced. For example, the Rn20-Rn100 pair ranges from 1.3 to 3 instead of 0 to 5. A more heterogeneous distribution of continental emissions would cause more frequent resetting and lead to an even narrower range in β.

5. 3-D Model

5.1. Model Description

The chemical tracer model (CTM) solves the continuity equations for a set of chemically reactive tracers over a global three-dimensional grid. The CTM is adopted from *Prather et al.* [1987]. In the present study the horizontal extension of a grid box is 8° in latitude and 10° in longitude. The atmosphere between Earth's surface and 10 hPa is divided into nine terrains following sigma layers centered, on average, at the pressure levels of 959, 894, 787, 635, 470, 322, 202, 110, and 40 hPa. The CTM uses a split-operator method to compute the separate effects of advection, dry and wet convection, large-scale diffusion, sources, and chemistry. The three processes of dynamical tracer redistribution are calculated with an 8-hour time step, while the time step for sources and chemistry is 1 hour. The advective transport of the tracer is upstream, conserving the second-order moments of the tracer distribution [*Prather*, 1986]. The meteorological data which are used as input for the CTM are provided by the Goddard Institute for Space Studies general circulation model II [*Hansen et al.*, 1983]. This data set contains 8-hour averages of mass flux, pressure fields, and convection frequencies as well as 5-day averages of temperature and detailed convection statistics for 1 year.

The three above mentioned tracers are also introduced into the 3-D model. These tracers have constant lifetimes of 5, 20, and 100 days, respectively, throughout the atmosphere and all seasons. Their source distribution is very simple: a uniform flux of 10^{14} molecules m^{-2} s^{-1} over all land areas north of 60°S for all three tracers and zero emissions elsewhere, in particular over the ocean. The emissions from coastal surface grid boxes are scaled to the proportion of land contained therein. Thus the tracers behave like the radioactive noble gas Radon, which is the reason for calling them Rn5, Rn20, and Rn100, respectively. Radon has a lifetime of 5.5 days and essentially continental (though much smaller) sources. In first approximation the tracers also behave like the alkanes, butane, propane, and ethane, which have also essentially continental (but not uniform) sources and comparable (but not constant) chemical lifetimes in the atmosphere. The fluxes mentioned above were selected to approximately match the global emission rate of ethane [cf. *Rudolph*, 1995] and amount to $7.1 * 10^{11}$ mol/year. The model was run for 1 full

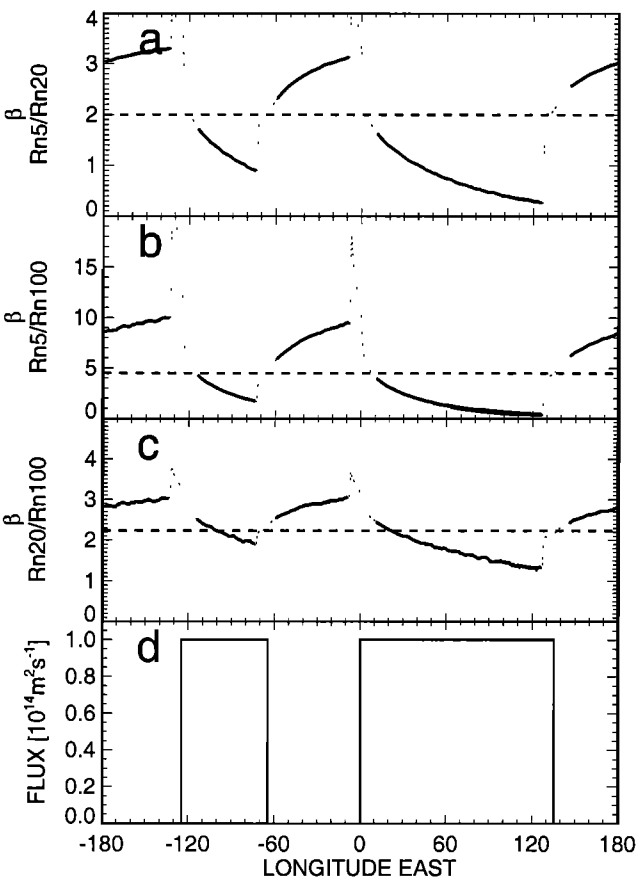

Figure 3. Slope β for the three possible pairs of the Rn tracers, (a) Rn5/Rn20, (b) Rn5/Rn100, and (c) Rn20/Rn100, as a function of longitude at 30°N-40°N latitude during March calculated with a 2-D advection-diffusion model. The dashed lines represent τ_j/τ_i and $\sqrt{\tau_j/\tau_i}$ with τ_j the lifetime of the longer-lived tracer of the pair. (d) Position of the continents.

year to reach steady state and was sampled the second year for the tracer distributions.

5.2. 3-D Model Results

To build on our insights gained from the 2-D advection diffusion model, we first consider the average surface concentrations generated by the 3-D model for the 32°N-40°N latitude belt during March (Figure 4). This latitude and month were chosen for the eventual comparison of the 3-D model results with the hydrocarbon distribution observed during the PEM West B campaign. The continents are placed at approximately the same longitudes as in the 2-D case although the source distribution in the 3-D model (Figure 4d) is more highly resolved and because of the varying coastline is more structured.

Just like the surface mixing ratios from the 2-D advection diffusion model the longitudinal distributions from the 3-D CTM show high values over the continents and low ones over the oceans. The maximum concentrations over the continents are slightly higher in the 3-D case but also scale like the square root of the tracer lifetime. However, in the 3-D model the distributions over the continents (and correspondingly over the oceans) are much more symmetrical. When averaged over a month, the changing wind patterns provide strong horizontal mixing which erodes the continental distribution from both ends, an effect which is missing in the 2-D model. Despite the diffusive horizontal mixing the concentrations over the remote oceans are significantly lower than in the 2-D case, indicating that in the 3-D case the air remains over the ocean longer. For each of the three tracers much of the horizontal gradients is concentrated in the coastal zones (about ±20° longitude with respect to the coast). This leaves a slightly ramped concentration plateau over the Eurasian continent and broad minima over the oceans, which divide surface air roughly into three categories: polluted continental air, background oceanic air, and air in the coastal transition zones.

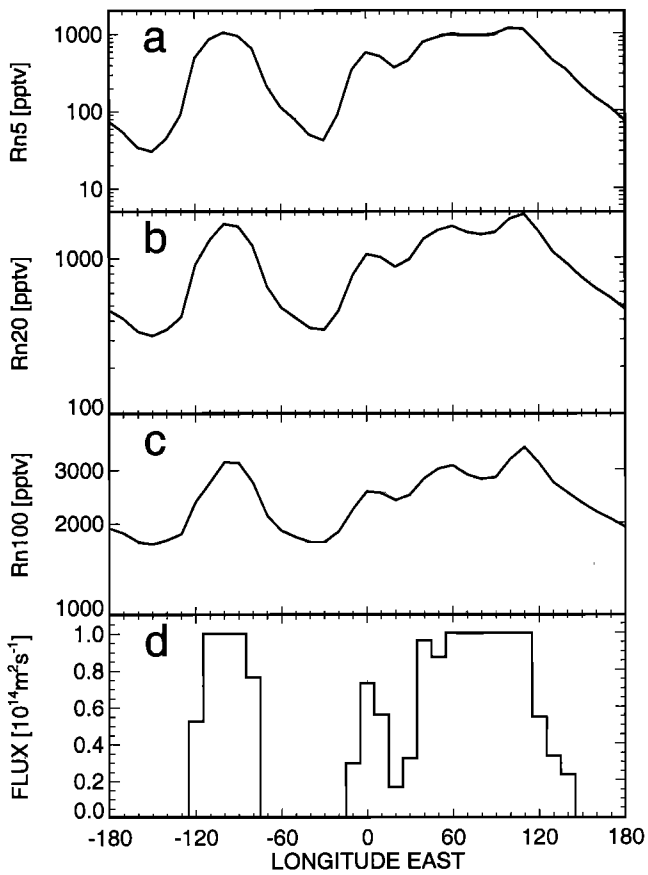

Figure 4. Surface mixing ratios of the synthetic tracers (a) Rn5, (b) Rn20, (c) Rn100 as a function of longitude at 32°N-40°N latitude during March calculated from the 3-D chemical tracer model. (d) Continental emission fluxes in that latitude band.

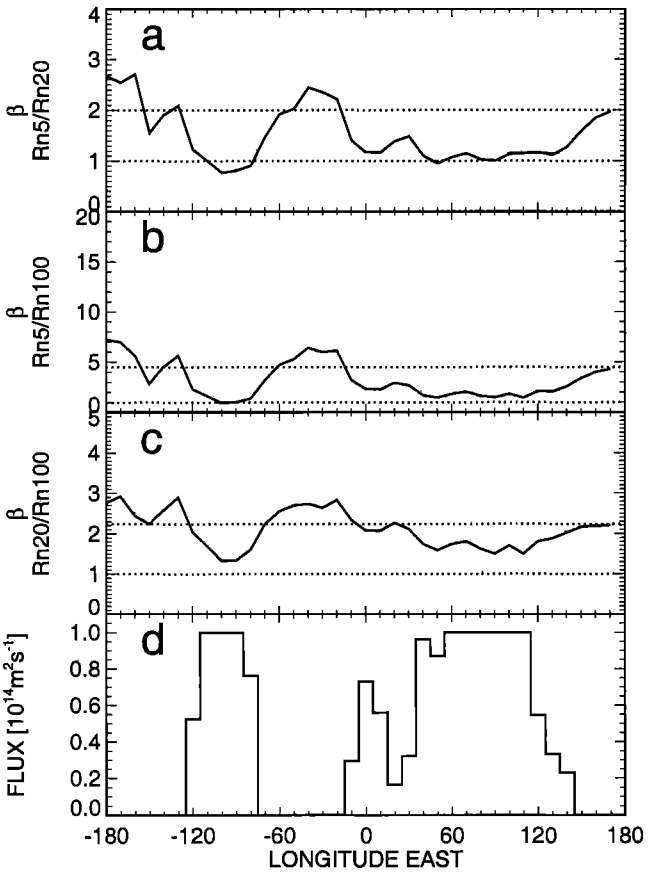

Figure 5. Slope β for the three possible tracer combinations as a function of longitude at 32°N-40°N latitude and the surface (0-0.4 km) during March calculated from the 3-D chemical tracer model. The dotted lines mark β values of 1 and $\sqrt{\tau_j/\tau_i}$. The lines for τ_j/τ_i coincide with the abscissas above. (d) Continental emission fluxes.

Figure 5, which presents the corresponding slope β, shows also considerable deviations from the 2-D case. First, in the 3-D case β does not approach zero as was observed in the 2-D case over the large Eurasian continent; instead, it hardly dips below 1. Second, its range is also significantly reduced with respect to the upper

bound. At continental longitudes it varies between 1 and $\sqrt{\tau_j/\tau_i}$; the latter is indicated by the upper dotted line in Figure 5a - 5c. Nevertheless, as in the 2-D case β is lower over the continents and higher over the oceans, where it clearly exceeds $\sqrt{\tau_j/\tau_i}$. The major gradients in β are located at the coastlines.

The numerical value of β tells us how important removal by mixing is with respect to chemical decay. A value of 1 indicates that the respective Rn concentrations correlate linearly. This means that their concentrations change at exactly the same rate and thus that their removal from surface air is essentially due to mixing, which acts on both tracers at the same rate. In the 3-D case this mixing in the continental near-surface air is essentially caused by the diurnal change in altitude of the boundary layer. At $\beta = \sqrt{\tau_j/\tau_i}$ transport and chemical removal act at about the same rate, as indicated by differential equation (4) for the 1-D diffusion, where transport by diffusion and chemical decay act on the tracer concentrations with the same rates as long as the system is in steady state. For $\beta > \sqrt{\tau_j/\tau_i}$ chemical decay is mostly responsible for local tracer removal.

The strong change of β in Figure 5 indicates that the plot of $\ln(\mathrm{Rn}_i)$ versus $\ln(\mathrm{Rn}_j)$ must be curved for concentrations sampled near the coastline. As Figure 6 shows, this is, indeed, the case. Over the continental sources, high mixing ratios prevail with a slope β close to 1. So the upper parts of the correlation curves in Figure 6 have tangents of slope 1. Since the range of concentrations over the continent is limited, that part of the curve is short. The middle part of the curve covers the transition zone where most of the decrease in concentration occurs; in that part the slope $\beta \approx \sqrt{\tau_j/\tau_i}$. Because the transition zone has the largest range of concentrations, that part of the correlation curve is relatively long. Over the remote ocean the concentration range becomes narrow again and approaches the slope $\beta \approx \tau_j/\tau_i$. That range forms the bottom part of the curve. An attempt of fitting linear regression lines to the full data ensembles is indicated by the dashed lines. The resulting slopes are close to $\sqrt{\tau_j/\tau_i}$. For comparison, Figure 6 shows the corresponding correlations between the surface mixing ratios of ethane, propane, and n-butane measured in the same region during PEM West B. Measurements and measurement domain are described by *Blake et al.* [1997] (see also section 6). Again, the resulting slopes are as close to $\sqrt{\tau_j/\tau_i}$ as can be derived from a comparison with the hydrocarbon lifetimes listed in Table 2. Incidentally, the slopes γ for the same data sets are 1.76 for the alkanes and 2.6 for the Rns in good agreement with the values $\frac{\sqrt{k_{nB}}-\sqrt{k_E}}{\sqrt{k_P}-\sqrt{k_E}}$ =1.91 and $\frac{\sqrt{1/\tau_{Rn5}}-\sqrt{1/\tau_{Rn100}}}{\sqrt{1/\tau_{Rn20}}-\sqrt{1/\tau_{Rn100}}}$ = 2.81 expected from (16) and (15).

The slopes β depend strongly on the absolute values of the tracer lifetimes, which makes the direct comparison between the β from different tracer pairs difficult. To remove most of that dependency, we normalize β to

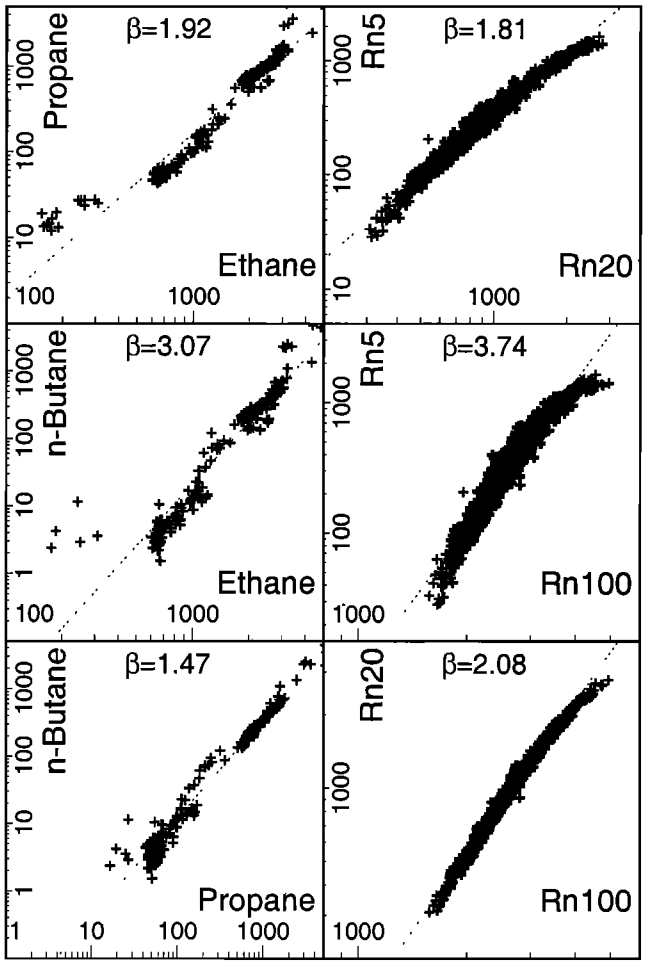

Figure 6. (right column) Correlations between the calculated surface (0-0.4 km) mixing ratios of the synthetic tracers in the domain 32°N-40°N latitude, 115°E-155°E longitude during March. (left column) For comparison the correlations between the surface (0-1 km) mixing ratios of ethane, propane, and n-butane measured in the same area during PEM West B are shown. The dashed lines represent linear fits to all data in a plot. Their slopes β are indicated.

the ratio of the lifetimes by introducing

$$\alpha_{ij} = ln(\beta_{ij})/ln(\tau_j/\tau_i) \tag{21}$$

or equivalently

$$\beta_{ij} = (\tau_j/\tau_i)^{\alpha_{ij}} \tag{22}$$

We note that a slope $\beta_{ij} = 1$ transforms into a $\alpha_{ij} = 0$; $\beta_{ij} = \sqrt{\tau_j/\tau_i}$ transforms into a $\alpha_{ij} = 1/2$; and $\beta_{ij} = \tau_j/\tau_i$ transforms into $\alpha_{ij} = 1$ regardless of the pair of τ_j/τ_i. In the following we will view the global distributions of the slopes in terms of α.

The global distributions confirm the conclusions derived from the longitudinal cross sections. Figure 7 presents first the latitude by longitude distributions of the surface concentrations of the three tracers averaged over the month of March [see *Ehhalt et al.*, 1997]. The contours of constant mixing ratio for all lifetimes follow

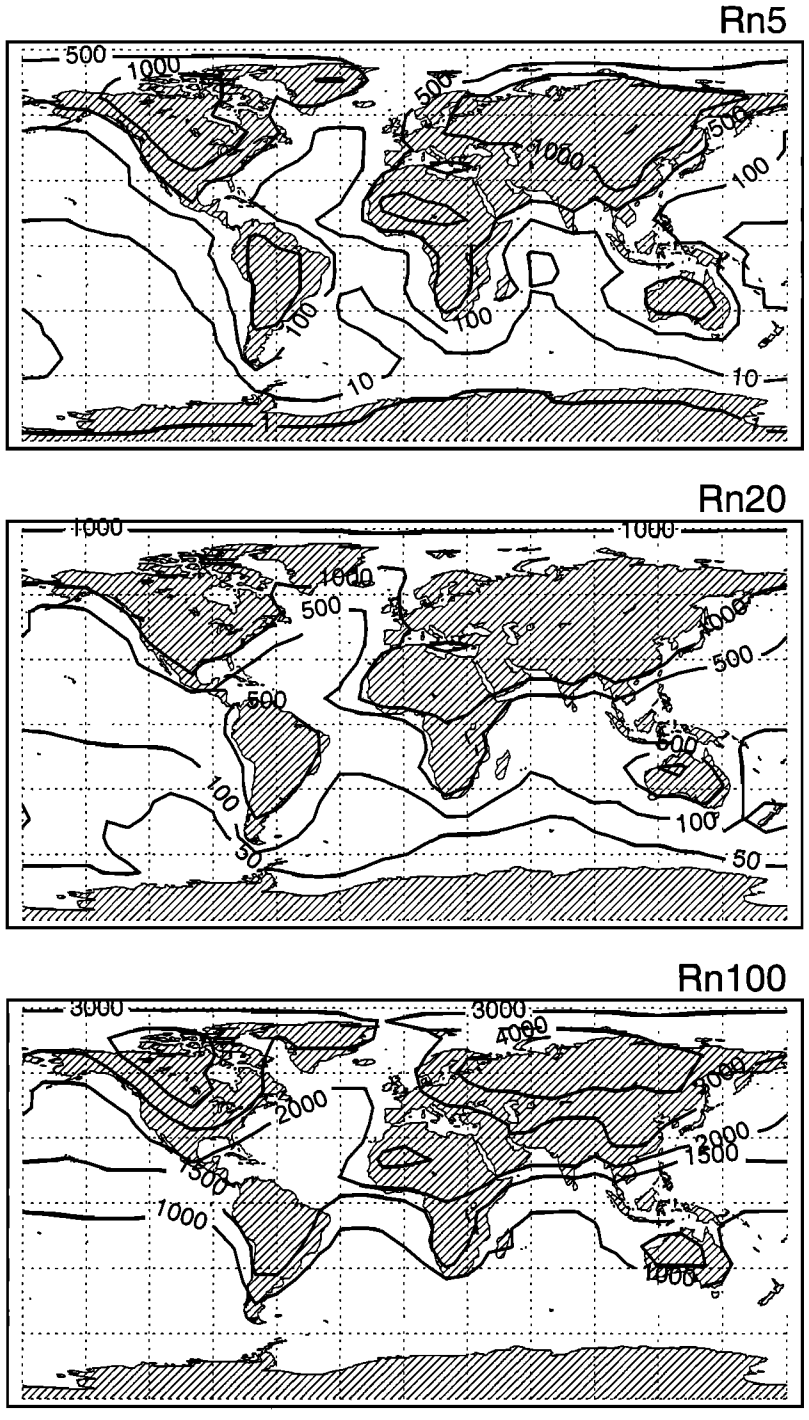

Figure 7. Average global surface (0-0.4 km) distribution of the synthetic tracers Rn5, Rn20, and Rn100 during March. The contours of constant mixing ratio are given in parts per trillion by volume.

the continental outline, where most of the horizontal gradient is concentrated. Superimposed is a latitudinal gradient, which is caused by the fact that most of the continental area, that is, most of the sources, is located in the northern hemisphere. That gradient is more strongly expressed for the longer-lived tracers, because their lifetimes become longer than that for zonal mixing, and longitudinal gradients are therefore relatively weaker. Corresponding distributions for higher altitudes (500 hPa and 200 hPa) are given by *Ehhalt et al.* [1997], and show even stronger latitudinal alignment of the isolines. Some memory of the continental surface sources, however, is retained in the contour lines at 200 hPa in the tropics and is caused by the strong and deep vertical convection at these latitudes.

The latitude by longitude distributions of α for the various pairs of tracers are shown in Plates 1 and 2 again averaged over the month of March. They were obtained

by first calculating the slopes β from plots of $\ln(\mathrm{Rn}_i)$ versus $\ln(\mathrm{Rn}_j)$ of the 24-hour averages in each grid box of the 3-D model, by converting these to α using relation (21), and then by applying a contour program. Values of α close to 0 are indicated by green colors, values around 1/2 are indicated by blue, and those close to 1 are indicated by red colors. An α of 0 means that the local tracer gradient is essentially caused by local mixing; for $\alpha = 1/2$, local transport and chemical loss are about equally responsible for the change in tracer concentration, and for $\alpha > 1/2$, local chemistry is causing most of the tracer removal.

The contour lines of α in the surface maps (Plates 1a to 1c) broadly confirm the findings from the longitudinal plots, namely, $\alpha \approx 0$ over the continents, a transition zone along the continental margins, and values approaching 1 over the middle of the ocean. Since the oceans make up a large part of the Earth's surfaces in the southern hemisphere, red colors dominate there. The patterns are approximately the same for the three tracer pairs but shifted toward higher α for Rn20/Rn100. The most likely reason is that the longer-lived tracers have vertical profiles that are less steep because of contributions from the other continents. Thus the mixing from the diurnal pumping of the boundary layer produces correlations over a much smaller range of concentrations than for the short-lived Rn5.

We also note that there are green colored areas away from the continental sources; despite the lack of sources and lower concentrations the local distribution over the ocean can be strongly influenced by local transport. We have not yet investigated what transport events are responsible for that finding, but it indicates that α may be a good diagnostic for mixing events in the model. This becomes even more apparent when we consider the higher altitudes (Plates 2a and 2b). At 500 hPa there is a broad band of fast local mixing over the equator and southern tropical latitudes. At 200 hPa we clearly see the upwelling in the tropical continents, a feature that is already visible in the mixing ratio contours themselves.

Thus the distributions of α provide a tool to visualize and investigate rates of transport in the model. Since within the model we can add additional tracers with other lifetimes and source distributions, α can be used as a diagnostic for a wide range of temporal and spatial scales of transport. Moreover, since the synthetic Rns are easy to introduce into most models, the α should be a good diagnostic for model intercomparison. This may prove a promising new application for tracer ratios. The more immediate question here is whether α or β can be used for the determination of the atmospheric lifetimes of hydrocarbons and thereby of the local OH concentration.

5.3. Dependence of α on the Chemical Lifetimes

Already the comparison between Plates 1a to 1c indicated that α not only depends on the geographical location but that the local α also depends on the chemical lifetimes of the two tracers considered. To investigate this point more closely, we consider the α within the area 32°-40°N latitude and 125°-145°E, that is, an area comprising two grid boxes in our 3-D CTM. It was also sampled during both the PEM West A and B campaigns. The α for the various pairs of synthetic tracers are listed in Table 1. They refer to the month of March and include also the tracers Rn1, Rn2, and Rn50 with lifetimes of 1, 2, and 50 days, respectively, in addition to those already mentioned.

Table 1 clearly demonstrates that the α_{ij} depend on the lifetimes of the tracers in a systematic way. The reasons for this systematic dependence become clearer when we consider the slope β in Figure 6. It is essentially given by the range of the values of $\ln(\mathrm{Rn}_i)$ divided by the range of the values of $\ln(\mathrm{Rn}_j)$. That range can also be characterized by the standard deviation of the Rn_i and Rn_j concentrations σ_i and σ_j. For easier comparison we use the relative standard deviation, $\sigma_i/\overline{M_i}$, where $\overline{M_i}$ represents the mean of the Rn_i concentration in the domain, and investigate its variation with $\ln(\tau_i)$ (Figure 8a). Clearly, there is a pronounced and systematic dependence of $\sigma_i/\overline{M_i}$ on the chemical lifetime τ_i. This dependence is related to that of α in the following manner: A straight line connecting any pair of data points in Figure 8a with τ_i and τ_j has the slope α_{ij} given in Table 1, in close approximation. Thus once it has been established that $\ln(M_i)$ and $\ln(M_j)$ correlate linearly, Figure 8a provides a more condensed representation of the information in Table 1.

Figure 8a can also be interpreted more readily. In terms of the mixing length hypothesis, $\sigma_i/\overline{M_i}$ is given by

$$\sigma_i/\overline{M_i} = l_i \times \frac{\nabla M_i}{\overline{M_i}} \tag{23}$$

where l_i is the mixing length and $\frac{\nabla M_i}{\overline{M_i}}$ is the mean logarithmic gradient of Rn_i. Both depend on τ_i but generally in opposite ways, which can generate a nonlinear behavior in $\sigma_i/\overline{M_i}$ such as that observed in Figure

Table 1. Values of $\alpha_{ij} = \ln(\beta_{ij})/\ln(\tau_j/\tau_i)$ for All Possible Pairs of Synthetic Tracers Rn_i and Rn_j in the Domain of 32°-40°N Latitude, 125°-145°E Longitude in the Month of March

	τ_i					
τ_j	100	50	20	5	2	1
100		0.50	0.46	0.37	0.33	0.31
50			0.41	0.33	0.29	0.26
20				0.25	0.21	0.17
5					0.084	0.03
2						-0.05
1						

Variable j denotes the longer-lived tracer.

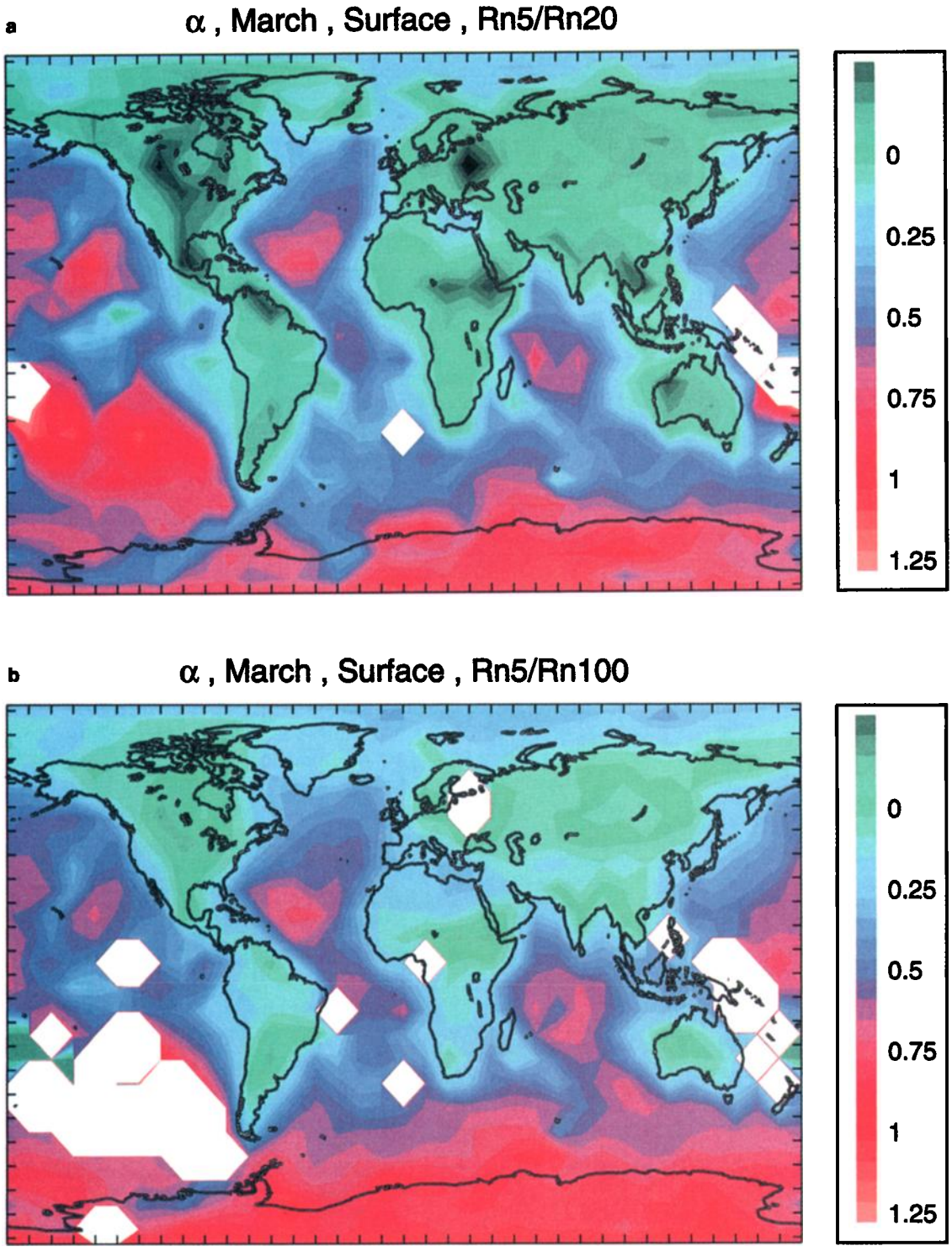

Plate 1. Global surface distribution of the exponent α for the different pairs of the synthetic tracers during March: (a) Rn5/Rn20, (b) Rn5/Rn100, and (c) Rn20/Rn100 (see equation (17) in text for the definition of α). The white areas indicate the regions where α is poorly defined due to large errors in β. The rejection is based on the correlation coefficient between $\ln(\mathrm{Rn}_i)$ and $\ln(\mathrm{Rn}_j)$ being less than 0.45.

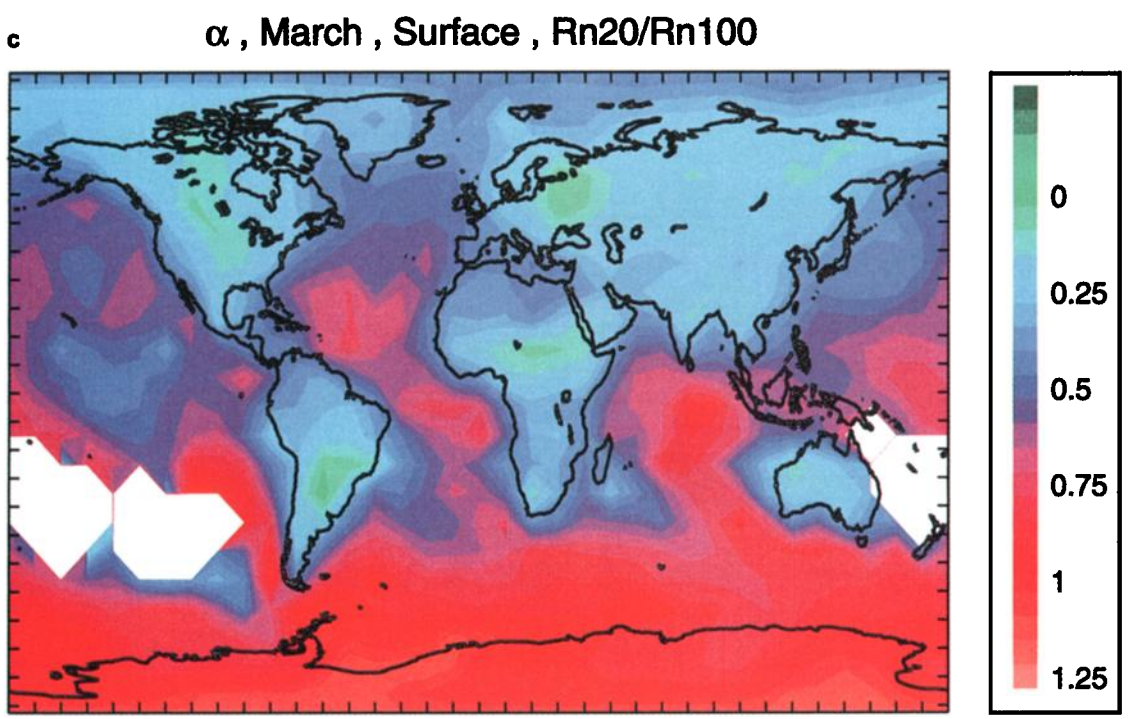

Plate 1. (continued)

8a. To illustrate that fact, the model-derived longitudinal gradient, $\frac{\partial M_i/\partial y}{\overline{M_i}}$, which is the major component of the gradient (see Figure 7), and the corresponding $l_i = \sigma_i/\frac{\partial M_i}{M_i \partial y}$ are also shown in Figure 8a as function of τ_i. The dependency of the former is quite plausible: a tracer with a shorter lifetime will decay more rapidly with time and thus with distance from the source and therefore exhibit steeper relative gradients (see Figure 7). We note, however, that the region represented by Figure 8a does contain sources. Their longitudinal gradient, which is depicted in Figure 5, also acts on the concentration gradient and may modify its dependence on τ_i. A similar argument holds for the mixing length. Because of decay the concentration an air parcel carries upon arrival at the point of observation corresponds to that of a location nearer than its origin. Consequently, the effective displacement length becomes smaller with shorter τ_i.

Since horizontal gradient and mixing length depend on the wind field, both vary in time and space and with them $\sigma_i/\overline{M_i}$. For example, the monthly average dependence of $\ln(\sigma_i/\overline{M_i})$ on $\ln(\tau_i)$ at the same location but for September is stronger by about 50% but has the same functional form. Locations farther removed from the sources even show a different functional form. For example, at 3 km altitude over the same area and at the surface at 165°-175°E longitude and 32°-40°N latitude, $\ln(\sigma_i/\overline{M_i})$ decreases nearly linearly with $\ln(\tau_i)$. More importantly, between 135°-155°E, and 32°-40°N, the area with the highest density of surface samples during PEM West B, the modeled $\ln(\sigma_i/\overline{M_i})$ over $\ln(\tau_i)$ shows an almost perfect linear relation (Figure 8b). The slope is -0.48 ± 0.01. It appears that at a given time interval and location the modeled $\sigma_i/\overline{M_i}$ exhibits a unique relationship with τ_i. Thus, within the model framework the function $\sigma/\overline{M}(\tau_i)$ can be used to determine the unknown lifetime τ_x of a tracer for which $\sigma_x/\overline{M_x}$ is known.

Obviously, a plot of the relative gradient, $\frac{\partial M_i}{M_i \partial y}$, versus $\ln(\tau_i)$, would serve the same purpose even better, because it is a monotonic function and would always yield a single value of τ_x for a given local value $\sigma_x/\overline{M_x}$ rather than two as in the first example. However the determination of a gradient requires sufficient data in at least two locations. These are often lacking when working with experimental data. Thus we prefer to work with $\sigma_i/\overline{M_i}$; especially since for many experimental examples, the curve $\ln(\sigma_i/\overline{M_i})$ over $\ln(\tau_i)$ is linear or at least monotonic (see below). It should be noted that *Junge* [1974] proposed a related approach. For globally averaged quantities he derived the relation

$$\sigma/\overline{M} = a \times \tau_i^{-b} \tag{24}$$

where the symbols σ, $\overline{M}$, and τ_i, have the same meaning as before and $a = 2.16 \times 10^{-2}$, when τ is given in years, and $b = 0.95$, that is close to 1. The constant b is equivalent to our α. Clearly, our regional analysis (see Figure 8a) can lead to a more complicated dependence of $\sigma/\overline{M}$ on τ_i than described by (24). Moreover, even when we obtain a regional solution in the form of (24), then the exponent b differs considerably from a value of 1. In the case of Figure 8b it has a value of 0.48; that is, $\sigma_i/\overline{M_i}$ is very close to a square root dependence on τ_i.

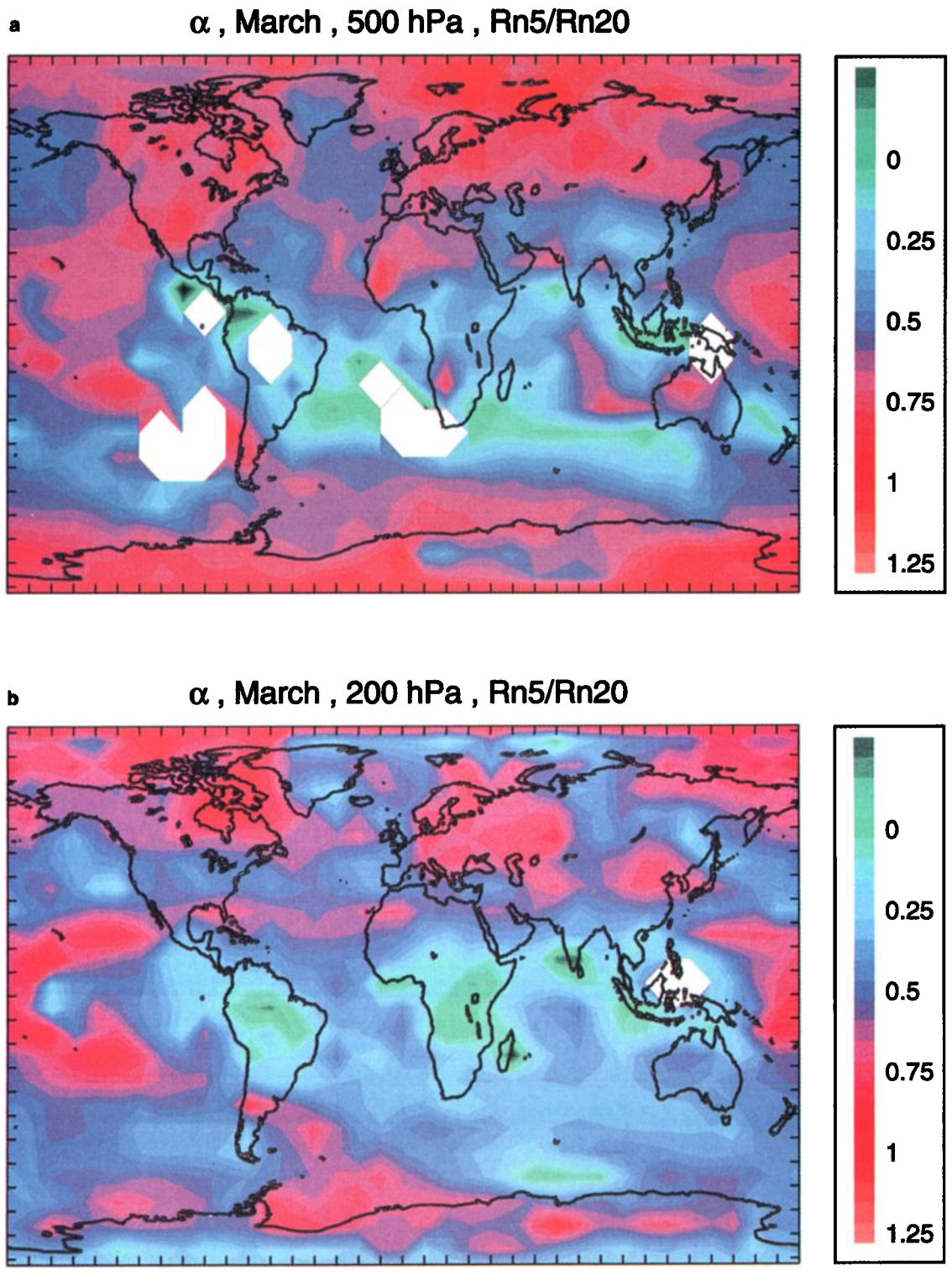

Plate 2. The global distribution of the exponent α for Rn5/Rn20 at (a) 500 hPa and (b) 200 hPa during March. The white areas indicate the regions where α is poorly defined due to large errors in β. The rejection is based on the correlation coefficient between $\ln(\mathrm{Rn}_i)$ and $\ln(\mathrm{Rn}_j)$ being less than 0.45.

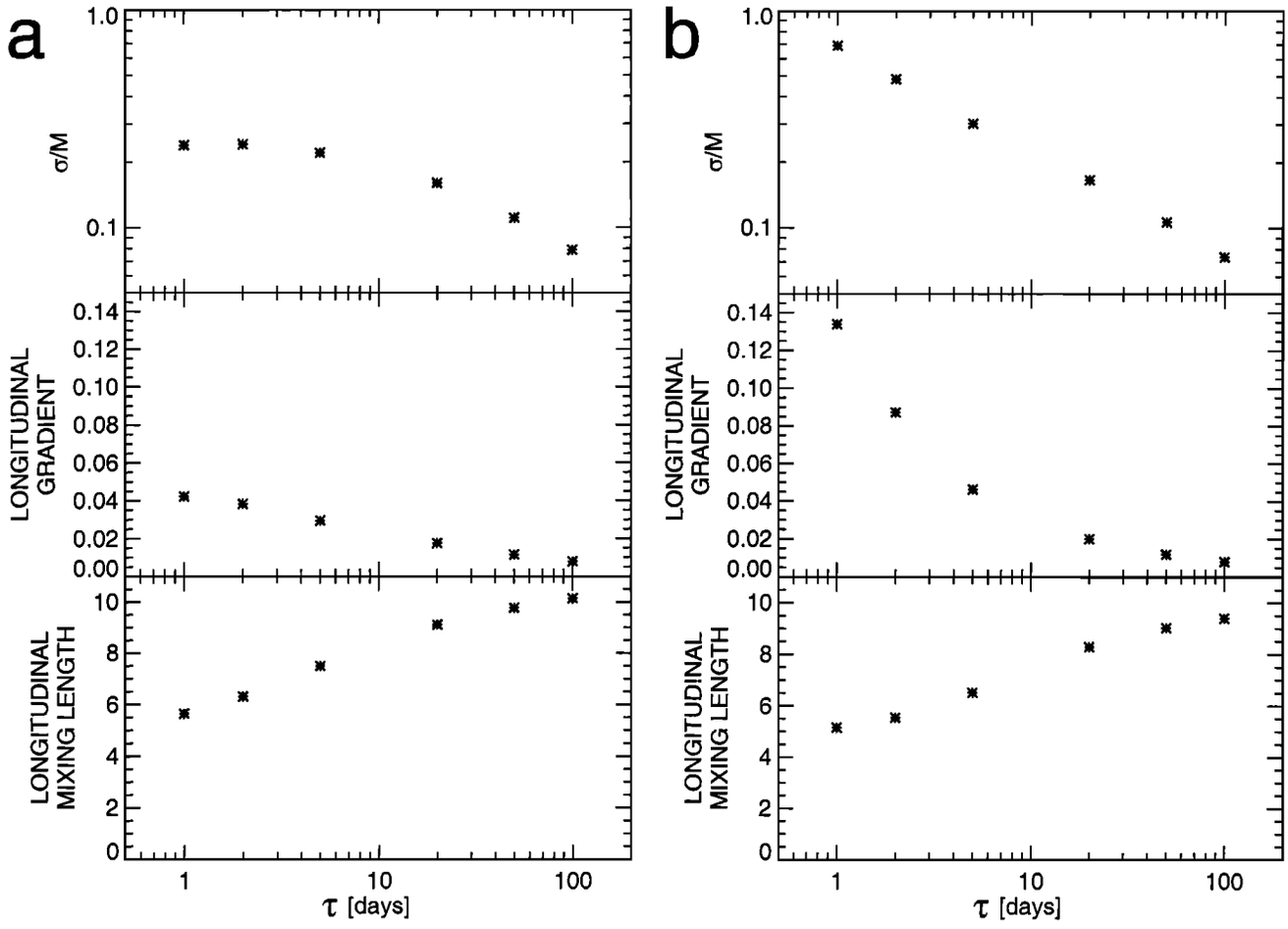

Figure 8. Average relative standard deviation of the synthetic tracers, relative longitudinal gradient (unit is degree^{-1}), and longitudinal mixing length (in degree longitude) as a function of the lifetime τ for the domain (a) 32°N-40°N latitude, 125°E-145°E longitude, and surface and (b) 32°N-40°N latitude, 135°E-155°E longitude, and surface during March.

6. Application to PEM West B Data

We will now try to apply the same principle to some of the experimental data from PEM West B. For that purpose we select the measurements of the hydrocarbons listed in Table 2 in the area 30°-40°N latitude and 134.8°-155°E longitude near the surface (0-1 km altitude). Excluding six highly polluted samples near Tokyo Airport, our data set consists of 49 samples each with significant concentrations for each of the listed hydrocarbons. The relative standard deviation, $\sigma_i/\overline{M_i}$, of these hydrocarbons is plotted against their rate constant, $k_{i,\mathrm{OH}}$, in Figure 9. In the logarithmic presentation of Figure 9 the data points for ethyne and the alkanes fall essentially on a straight line. The full curve is a least squares fit to these points. For these gases, which react exclusively or very nearly so with OH, Figure 9 also represents a plot of $\sigma_i/\overline{M_i}$ against the lifetime since $\log(\tau_i)$ = -$\log(k_{i,\mathrm{OH}})$ -$\log([\mathrm{OH}])$, where $\log([\mathrm{OH}])$ = const merely provides an offset. Clearly, the experimental $\sigma_i/\overline{M_i}$ also exhibit a unique relationship with $k_{i,\mathrm{OH}}$ and τ_i. Because $\log(\sigma_i/\overline{M_i})$ over $\log(\tau_i)$ also forms a straight line, the exponent α as defined in (15) assumes the same value for all pairs of hydrocarbons. The $\alpha = 0.49 \pm 0.03$ and is identical with the slope of the solid line in Figure 9. Unfortunately, because of the common and unknown factor [OH], the τ_i cannot be determined from this relationship alone. Additional information is needed, preferably in the form of simultaneous concentration measurements of a tracer with a known lifetime. Natural ^{222}Rn with a radioactive decay time $\tau = 5.5$ days provides such a tracer. It has the added advantage that like the alkanes it has essentially continental sources, and thus we may assume a similar source distribution at least on a large scale. Knowing $\sigma_{\mathrm{Rn}}/\overline{M_{\mathrm{Rn}}}$ and using the fitted line, one could assign a fictitious rate constant $k_{\mathrm{Rn,OH}}$ to the Rn data point and from it calculate [OH]:

$$[\mathrm{OH}] = \tau_{\mathrm{Rn}}^{-1} \times k_{\mathrm{Rn,OH}}^{-1} \tag{25}$$

Unfortunately, such Rn data are currently not available for PEM West B. Nonetheless, the combination of ^{222}Rn with hydrocarbon measurements appears to hold promise as a tool for deriving OH concentrations in future campaigns in similar geographic locations.

Table 2. Hydrocarbon Species Used in Figure 9 Together With Their Rate Constants k_{OH} for Reaction With OH at Room Temperature and an Approximate Lifetime Against Reaction With OH Assuming an Average OH Concentration of 10^6 cm^{-3}

Species	$k_{i,OH}$(298 K), 10^{12} cm^3 s^{-1}	τ_i, days
Ethane	0.254	46
Ethyne	0.767	15
Propane	1.12	10
i-Butane	2.19	5.3
n-Butane	2.44	4.7
i-Pentane	3.7	3.1
n-Pentane	4.0	2.9
n-Hexane	5.45	2.1
Ethene	8.52	1.4
Propene	26.3	0.44

Rate constants are from *Atkinson et al.* [1997]. Ethene and Propene react also with O_3; the rate constants at 298 K are 1.59×10^{-18} and 1.01×10^{-17}cm^3 s^{-1}, respectively.

A presently workable approach to derive [OH] from $\sigma_i/\overline{M_i}$ is to include a trace gas whose lifetime depends partly on the reaction with ozone, such as the alkenes, ethene, and propene which react with O_3 as well as OH and which also have been measured during PEM West B. In analogy to the procedure for ^{222}Rn we first assign fictitious rate constants, k'_E and k'_P, to ethene and propene, respectively, pretending that the alkenes react only with OH. The values of these are read from the fitted straight line in Figure 9 at $\sigma_E/\overline{M_E}$, $\sigma_P/\overline{M_P}$. We then relate the fictitious reaction rate with OH to the correct rate, which includes the reaction with O_3, for example,

$$k'_P \times [OH] = k_{P,OH} \times [OH] + k_{P,O_3} \times [O_3] = \tau_P^{-1} \quad (26)$$

and deduce

$$[OH] = \frac{k_{P,O_3}}{k'_P - k_{P,OH}} \times [O_3] \quad (27)$$

Adopting a value of 40 ppbv for the average O_3 concentration in the considered region [see *Crawford et al.*, 1997] and the rate constants given in Table 2, we derive an OH concentration of $(6^{+5.6}_{-2.0}) \times 10^5$cm^3 from the fictitious rate constant $k'_P = (4.33^{+0.92}_{-0.82}) \times 10^{-11}$ cm^3 s^{-1} for propene. We note that the error of the estimated OH concentration is large, owing to the error in k'_P. That error was obtained from the error in $\sigma_P/\overline{M_P}$ given in Figure 9, which, in turn, was estimated from the standard deviation of the alkane data from the fitted straight line. The error in the slope of the straight line contributes little to the total error. Nevertheless, propene does allow a significant estimate of the diurnally averaged [OH]. It is within the range theoretically expected for 35°N latitude and early March.

As a consequence of the low reactivity of ethene with O_3, the difference, $k'_E - k_{OH,E}$, in the denominator of (27) is small. Thus the error in the [OH] value derived from ethene becomes exceedingly large, despite the fact that the relative error in $k'_E = (9.05^{+1.91}_{-1.73}) \times 10^{-12}$ cm^3 s^{-1} is not larger than that of k'_P. The lower 1σ error bound of the estimated [OH] is 6.5×10^5 cm^{-3}, the upper is ∞ (the nominal value is, in fact, negative). Thus the consideration of ethene does not provide a useful central value for [OH] but only a lower bound.

7. Conclusion and Summary

In the foregoing approach we essentially used measured data and empirical relations between the data.

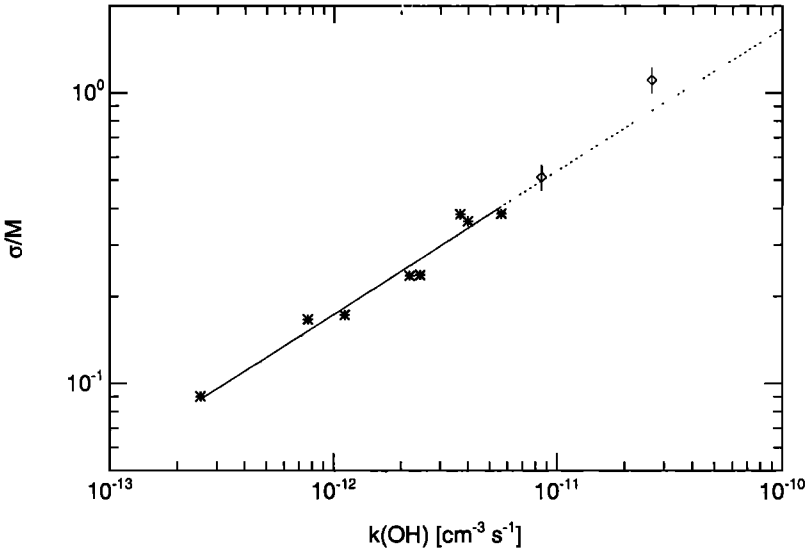

Figure 9. Average relative standard deviation of the hydrocarbons measured during PEM West B in the domain 30°N-40°N latitude, 135°E-155°E longitude, and surface (0-1 km) as a function of their reaction rate constant k_{OH} with OH. The rate constants are given in Table 2. Diamonds symbolize the alkenes; the asterisks symbolize ethyne and the alkanes. The straight line represents a linear fit to the latter.

We tried to minimize the use of additional information or model assumptions in the hope of keeping the systematic errors small. Thus there is no need to postulate a mixing mechanism nor to guess the background concentrations, as would be required for the traditional approach that leads to solutions (1) and (8) described in section 2. This also reduces the possibility of systematic errors in the derived [OH] which are introduced by these assumptions. Nevertheless, we had to make some assumptions. To derive the fictitious k', we had to assume that the straight line fitted to the alkane data extrapolated linearly to the larger k_{OH} (or shorter τ). As we showed for the modeled results, this does not need to be the case. However, the model data for the selected area and month (Figure 8) do yield an almost perfect linear relation between $\ln(\sigma_i/\overline{M_i})$ and $\ln(\tau_i)$. Moreover, the measured hydrocarbon data for that area including those for ethene and propene, the latter together with a reasonable assumption about the possible contribution from the reaction with O_3 to their lifetime, fall on a straight line. So we do not expect a large systematic error from that side.

Other assumptions required by the present technique are also needed by the traditional approach. The first is that of equal source distributions for the hydrocarbons. This is not strictly true, even if we assume the same continental source distributions for the considered hydrocarbons. The oceans are a minor but not negligible source of alkenes. This is much less so for the alkanes. Thus the respective source distributions are not exactly the same, which might become significant for samples taken over the remote ocean, where the oceanic source would tend to prevent very low values of the alkenes and thus reduce the variance in their concentration. This, in turn, would result in smaller fictitious rate constants and thus higher estimates in [OH]. Since the locations sampled here are sufficiently close to the very strong continental sources, we would expect their influence to dominate the variances observed, and thus there would be little influence from the oceanic source.

A similar effect can be caused by a possible contamination of the samples by alkenes generated at the walls of the sample flasks, a problem which has plagued early alkene measurements. From the linear correlations of the log of the ethene and propene mixing ratios against the alkanes it appears that this was not a source of concern for the present data.

The next assumption is that there are no other oxidants reacting with the alkanes or alkenes in a significant way, notably the nitrate radical and halogen atoms. None of these species have been measured during PEM West B. However an influence of the former can be excluded on the basis of the low NOx concentrations found over the considered domain during PEM West B [*Kondo et al.*, 1997]. The concentrations of the latter outside the polar regions are generally considered to be too low for a significant impact [*Rudolph et al.*, 1997]. Again, correlation plots of the alkene and alkene/alkane mixing ratios can be used to detect the influence of such reactions.

Since the assumptions needed for the present approach are fewer and partly different than those needed for the traditional approach, it would be interesting to apply both techniques to the same data set. It would allow some insight into the magnitude of the so far unknown systematic errors introduced by the different assumptions of the various approaches. Since the latter also requires the knowledge of the average travel time from the coast to the point of observation as derived from trajectory analyses, for example, which are at present not available to us, this remains a future task.

We investigated the average near-surface distribution of trace gases with the same emission patterns but different atmospheric lifetimes. We showed that in the presence of diffusive mixing the rate of dilution depends on the chemical lifetime of the gas. In the 1-D and 2-D cases studied, this dependence is explicit in the analytical solutions presented; in the 3-D case provided by a chemical tracer model, this is shown implicitly by the fact that the horizontal mixing length depends on τ_i, which, in turn, will influence the rate of horizontal eddy diffusion.

This finding has several implications. First, for the cases studied the function describing the spatial and temporal distributions of the trace gases cannot be separated into two factors: one describing transport and the other describing the chemical loss. Second, it changes the interpretation of the slopes in the correlations of trace gas mixing ratios or of ratios of mixing ratios. Over a wide geographical range these ratios depend on $\sqrt{\tau_i}$. Third, in these situations the traditional way of determining τ and [OH] from pairs of hydrocarbons may fail.

Nevertheless, one can derive procedures to derive these quantities from sets of hydrocarbon measurements. The most simple procedure is to relate $\ln(\sigma_i/\overline{M_i})$ to $\ln(\tau_i)$. In the most favorable cases this leads to a linear relation, that is, $\sigma_i/\overline{M_i} = A \times \tau_i^{-\alpha}$, where $\alpha \approx 1/2$. In any case this procedure leads to a unique function $\sigma_i/\overline{M_i}$ of τ_i. To use this procedure for the determination of [OH], additional information is needed. In the present case this is provided by the alkenes, whose lifetime is partly determined by reaction with O_3 (of known concentration). Thus we derived an OH concentration of $6 \times 10^5 \mathrm{cm}^{-3}$ for the PEM West domain of 30°-40°N latitude, 135°-155°E longitude during early March. The estimated 1σ error is a factor of 2. A major assumption remains, namely, that of a similar source distribution for the tracers considered. A byproduct is the global distribution of α which appears to provide a convenient indicator of tracer mixing on a regional scale.

References

Atkinson, R., D.L. Baulch, R.A. Cox, R.F. Hampson, J.A. Kerr, M.J. Rossi, and J. Troe, Evaluated kinetic, photo-

chemical and heterogeneous data for atmospheric chemistry, supplement V, IUPAC subcommittee on gas kinetic data evaluation for atmospheric chemistry, *J. Phys. Chem. Ref. Data, 26*, 521-1011, 1997.

Bamber, D.J., P.G.W. Healey, B.M.R. Jones, S.A. Penkett and A.F. Tuck, Vertical profiles of tropospheric gases: chemical consequences of stratospheric intrusions, *Atmos. Environ. 18,* 1759-1766, 1984.

Blake, N., S.A. Penkett, K.C. Clemitshaw, P. Anwyl, P. Lightman, and A.R.W. Marsh, Estimates of atmospheric hydroxyl radical concentrations from the observed decay of many reactive hydrocarbons in well-defined urban plumes, *J. Geophys. Res., 98,* 2851-2864, 1993.

Blake, N.J., D.R. Blake, T.-Y. Chen, J.E. Collins Jr., G.W. Sachse, B.E. Anderson, and F.S. Rowland, Distribution and seasonality of selected hydrocarbons and halocarbons over the western Pacific basin during PEM-West A and PEM-West B, *J. Geophys. Res., 102,* 28,315-28,331, 1997.

Bonsang, B., M. Kanakidou, and G. Lambert, Nonmethane hydrocarbons chemistry in the atmosphere of an equatorial forest: A case study of indirect photochemical production of OH radicals, *Geophys. Res. Lett., 14*, 1250-1253, 1987.

Calvert, J.G., Hydrocarbon involvement in photochemical smog formation in Los Angeles atmosphere, *Environ. Sci. Technol., 10*, 256-262, 1976.

Crawford, J., et al., An assesment of ozone photochemistry in the extratropical western North Pacific: Impact of continental outflow during the late winter/early spring. *J. Geophys. Res., 102*, 28,469-28,487, 1997.

Ehhalt, D.H., F. Rohrer, A.B. Kraus, M.J. Prather, D.R. Blake, and F.S. Rowland, On the significance of regional trace gas distribution as derived from aircraft campaigns in PEM West A and B, *J. Geophys. Res., 102*, 28,333-28,351, 1997.

Hansen, J., G. Russel, P. Stone, A. Lacis, S. Lebedeff, R. Ruedy, and L. Travis, Efficient three-dimensional global models for climate studies: Models I and II, *Mon. Weather Rev., 111*, 609-662, 1983.

Junge, C.E., Residence time and variability of tropospheric trace gases, *Tellus, 26*, 477-488, 1974.

Kondo, Y., M. Koike, S. Kawakami, H.B. Singh, H. Nakajima, G.L. Gregory, D.R. Blake, G.W. Sachse, J.T. Merrill, and R.E. Newell, Profiles and partitioning of reactive nitrogen over the Pacific Ocean in winter and early spring, *J. Geophys. Res., 102*, 28,405-28,424, 1997.

Kramp, F., and A. Volz-Thomas, On the budget of OH radicals and ozone in an urban plume from the decay of C5-C8 hydrocarbons and NOx, *J. Atm. Chem., 28*, 263-282, 1997.

McKeen, S.A., M. Trainer, E.Y. Hsie, R.K. Tallamraju, and S.C. Liu, On the indirect determination of atmospheric OH radical concentrations from reactive hydrocarbon measurements, *J. Geophys. Res., 95*, 7493-7500, 1990.

McKeen, S.A., S.C. Liu, E.-Y. Hsie, X. Lin, J.D. Bradshaw, S. Smyth, G.L. Gregory, and D.R. Blake, Hydrocarbon ratios during PEM-WEST A: A model perspective, *J. Geophys. Res., 101*, 2087-2109, 1996.

McKenna, D.S., C.J. Hord, and J.M. Kent, Hydroxyl radical concentrations and Kuwait oil fire emission rates for March 1991, *J. Geophys. Res., 100*, 26,005-26,026, 1995.

McKenna, D.S., Analytic solutions of reaction diffusion equations and implications for the concept of an air parcel, *J. Geophys. Res., 102*, 13,719-13,725, 1997.

Nelson, P.F., and S.M. Quigley, Non-methane in the atmosphere of Sydney, Australia, *Environ. Sci. Technol., 16*, 650-655, 1982.

Prather, M.J., Numerical advection by conservation of second-order moments, *J. Geophys. Res., 91*, 6671-6681, 1986.

Prather, M.J., M.B. McElroy, S.C. Wofsy, G. Russel, and D. Rind, Chemistry of the global troposphere: Fluorocarbons as tracers of air motion, *J. Geophys. Res., 92*, 6579-6613, 1987.

Roberts, J.M., F.C. Fehsenfeld, S.C. Liu, M.J. Bollinger, C. Hahn, D.L. Albritton, and R.E. Sievers, Measurements of aromatic hydrocarbon ratios and NOx concentrations in the rural troposphere: Observations of air mass photochemical aging and NOx removal, *Atmos. Environ., 18*, 2421-2432, 1984.

Roberts, J.M., R.S. Hutte, F.C. Fehsenfeld, D.L. Albritton, and R.E. Sievers, Measurements of anthropogenic hydrocarbon concentration ratios in the rural troposphere: Discrimination between background and urban sources, *Atmos. Environ., 19*, 1945-1950, 1985.

Rudolph, J., The tropospheric distribution and budget of ethane, *J. Geophys. Res., 100*, 11,369-11,381, 1995.

Rudolph, J., and F.J. Johnen, Measurements of light atmospheric hydrocarbons over the Atlantic in regions of low biological activity, *J. Geophys. Res., 95*, 20,583-20,591, 1990.

Rudolph, J., B. Ramacher, C. Plaß-Dülmer, K.-P. Müller, and R. Koppmann, The indirect determination of chlorine atom concentration in the troposphere from changes in the patterns of nonmethane hydrocarbons, *Tellus, 49B*, 592-601, 1997.

Singh, H.B., J.R. Martinez, D.G. Hendry, R.J. Jaffe, and W.B. Johnson, Assessment of the oxidant-forming potential of light saturated hydrocarbons in the atmosphere, *Environ. Sci. Technol., 15*, 113-119, 1981.

D.R. Blake, Department of Chemistry, University of California, Irvine, Irvine, CA 92717. (e-mail dblake@orion.oac.uci.edu)

D.H. Ehhalt, F. Rohrer, and A. Wahner, Institut für Atmosphärische Chemie, Forschungszentrum Jülich, 52425 Jülich, Germany. (e-mail f.rohrer@fz-juelich.de, a.wahner@fz-juelich.de)

M.J. Prather, Department of Earth System Science, University of California, Irvine, Irvine, CA 92717. (e-mail mprather@uci.edu)

(Received November 19, 1997; revised March 26, 1998; accepted March 31, 1998.)